How small-molecule inhibitors of dengue-virus infection interfere with viral membrane fusion

Luke H. Chao[1]*, Jaebong Jang[3], Adam Johnson[1], Anthony Nguyen[1], Nathanael S. Gray[3], Priscilla L. Yang[4], Stephen C. Harrison[1,2†]

[1]Department of Biological Chemistry and Molecular Pharmacology and [2]Howard Hughes Medical Institute, Harvard Medical School, Boston MA 02115

[3]Department of Cancer Biology, Dana-Farber Cancer Institute and Department of Biological Chemistry and Molecular Pharmacology, Harvard Medical School, Boston, MA 02115

[4]Department of Microbiology and Immunobiology, Harvard Medical School, Boston, MA 02115

*Current address: Department of Molecular Biology, Massachusetts General Hospital, Department of Genetics, Harvard Medical School, Boston, MA 02114

†Correspondence: harrison@crystal.harvard.edu

Abstract

Dengue virus (DV) is a compact, icoshedrally symmetric, enveloped particle, covered by 90 dimers of envelope protein (E), which mediates viral attachment and membrane fusion. Fusion requires a dimer-to-trimer transition and membrane engagement of hydrophobic "fusion loops". We previously characterized the steps in membrane fusion for the related West Nile virus (WNV), using recombinant, WNV virus-like particles (VLPs) for single-particle experiments. Trimerization and membrane engagement are rate-limiting; fusion requires at least two adjacent trimers; availability of competent monomers within the contact zone between virus and target membrane creates a trimerization bottleneck. We have extended that work to dengue VLPs, from all four DV serotypes, finding an essentially similar mechanism. Small-molecule inhibitors of DV infection that target E block its fusion-inducing conformation change. We show that ~15 bound molecules per particle (~8.5 % occupancy) completely prevent fusion, in accord with the proposed mechanism and the likely inhibitor binding site on E.

Impact statement

Single-particle studies of dengue-virus membrane fusion and the effect of small-molecule inhibitors of infection clarify the viral fusion mechanism.

Introduction

Flaviviruses, a family that includes dengue, tick-borne encephalitis, West Nile, and Zika viruses, are a group of mosquito-borne pathogens of substantial interest for vaccine and small molecule therapeutic development (Diamond and Pierson, 2015; Heinz and Stiasny, 2012). The envelope glycoprotein (E) is the membrane fusogen required for cell entry and infection (Harrison, 2015). E comprises three beta-sheet rich domains: domain I is a central beta barrel that organizes the rest of the subunit; domain II (an extension emanating from domain I) bears a hydrophobic fusion loop at its distal tip; domain III, with an immunoglobulin-like fold, connects to the C-terminal "stem" and transmembrane helical hairpin (Rey et al., 1995). The conserved, fusion-inducing conformational rearrangements these proteins undergo when exposed to reduced pH, from a pre-fusion dimer to a post-fusion trimer, offer an opportunity to exploit the common structural features of all flavivirus E proteins to find viral entry inhibitors.

In a crystal structure of the dengue serotype 2 E dimer, a molecule of β-octyl glucoside (β-OG), used in the preparation, was present in a pocket between domains I and II (Modis et al., 2003). This pocket closes up during the fusogenic conformational change (Modis et al., 2004), and the observation that a small molecule can bind there suggested that it might be a good target for an entry inhibitor. Indeed, a screen originally designed to detect small molecules that interfere with another step in the conformational transition yielded a series of cyanohydrazone compounds subsequently shown to bind at or near the β-OG pocket (Clark et al., 2016; Schmidt et al., 2012). These compounds block fusion *in vitro* and infection in cell culture; they bind the dimer on the virion surface before the virus attaches to a cell. The most potent of them inhibit viral infectivity with IC_{90} values in the single-digit micromolar range (Schmidt et al., 2012).

In previous work on the mechanism of membrane fusion by West Nile virus (WNV) E, we used single-particle fusion measurements with WNV virus-like particle (VLPs) to outline steps in the transition leading to membrane merger (Chao et al., 2014). We could interpret the observed, pH-dependent kinetics with a model in which trimerization of E into an extended intermediate, with the three fusion loops inserted into the target membrane, becomes a kinetic bottleneck in progression to hemifusion, because hemifusion requires collapse to the postfusion conformation of at least two *adjacent* trimers in the contact zone between a virus particle and the membrane with which it is fusing. Stochastic simulations gave estimates for the rates of various steps. In the present work, we have extended the analysis to all four dengue virus (DV) serotypes, using VLPs as in our studies of WNV fusion. We also use this approach to determine the mechanism of inhibition by compounds in the cyanohydrazone series and to estimate the number of small-molecule inhibitors per particle needed to block fusion.

Results

Single-particle measurement of dengue VLP hemifusion kinetics

VLPs for the four DV serotypes were prepared by expression in 293T cells, essentially as described for WNV VLPs (Chao et al., 2014). Expression was at 28°C rather than 37°C, as the latter yielded particles with substantially lower fusion activity. We measured the pH

dependence of bulk hemifusion and found sharply sigmoidal curves with inflection pH of 6.1 for the DV4 VLPs and ~5.4 for those of DV1, DV2 and DV3 (Fig. 1A). We used total internal reflection fluorescence microscopy as described previously (Chao et al., 2014; Floyd et al., 2008; Ivanovic et al., 2013; Kim et al., 2017) to determine single-particle dwell time distributions for hemifusion at pH 5.5 (Fig. 1B), with dequenching of DiD-labeled VLPs to mark the moment of hemifusion with the supported lipid bilayer. We incorporated into the target bilayer a pseudo-receptor, to uncouple membrane attachment from exposure of the fusion loop triggered by the pH drop. The receptor was either the lectin domain of DC-SIGN-R linked through a histidine tag to a NiNTA-headgroup lipid or a similarly linked, antigen-binding fragment (Fab) from antibody 1AID-2, specific for DV2 domain II (Chao et al., 2014; Lok et al., 2008; Tassaneetrithep et al., 2003). We found no receptor-dependence of hemifusion dwell times; the data shown are with the DC-SIGN-R.

The dwell-time distributions in Fig. 1B show some differences among the four serotypes. The exponential used to fit the distributions for DV1, DV2 and DV4 VLPs gives an effective rate constant for a first-order "rate-limiting step"; the best formal fit for DV3 includes two successive or parallel steps, but the sampling is too limited to draw strong conclusions. The bulk fusion vs. pH curve is also less sharply sigmoidal than are the others. Although the inflection pH measured in bulk is similar for DV1, DV2 and DV3, the effective first-order rate of fusion for DV1 is slower.

Small-molecule inhibition

The compound 3-110-22 (Fig. 2) inhibits DV2 infection with IC_{90} of 0.7 μM (Schmidt et al., 2012). The IC_{50} for DV2 VLP fusion, measured in bulk, was 1-2 μM (Fig. 2A). We used a concentration of 1 μM to study the effect of 3-110-22 on the dwell-time distribution for single-particle fusion at pH 5.5 (Fig. 2B). Comparison of Fig. 2B with the DV2 VLP panel in Fig. 1B shows that presence of the inhibitor has spread the distribution and introduced a clear rise and fall, suggesting that the inhibitor has retarded a step other than the one that is effectively rate-limiting in its absence. Our simulation for the DV2 VLP fusion reaction, described below, dissects the mechanism into steps of conformational change in E and gives results consistent with the β-OG pocket as the site of 3-110-22 interaction.

To relate single-particle hemifusion dwell-time distribution and small-molecule occupancy, we conjugated a fluorescent probe (Alexa-555) to 3-110-22 at the 4-position of the benzene ring (see Methods). We confirmed that the modified form of the inhibitor was active by recording bulk hemifusion inhibition and found its IC_{50} to be about 10- to 20-fold higher that of the unmodified compound; the strong tendency of these hydrophobic compounds to associate in solution reduces the effective monomer concentration, and the actual difference may be smaller (Fig. S2A, Supplement to Fig. 2). We also showed that 3-110-22 competed for binding with the modified inhibitor, indicating that they both interact at the same site (Fig. S2B, Supplement to Fig. 2).

We incubated DV2 VLPs with 1 μM Alexa-555/3-110-22, removed excess compound with a desalting column (Schmidt et al., 2012), and measured single-particle hemifusion events. We determined inhibitor occupancy for each particle using a calibrated intensity in the Alexa-555 channel (see Methods) and correlated the occupancy with hemifusion fate of that particle. At pH 5.5 under the conditions of our experiment, the overall yield of hemifusion in the absence

of inhibitor was ~25% (i.e., the percent of total particles in the observation field that ultimately fused). Particles with more than about 12 bound inhibitors failed to fuse at all (Fig. 3). We did not detect particles with more than about 60 copies of Alexa-555/33-110-22, showing that binding saturated at an occupancy consistent with a large fraction of "small VLPs" (60 E subunits).

Simulation of DV2 fusion and inhibitor mechanism

We modeled the conformational steps preceding hemifusion with a stochastic simulation, structured like the scheme we used for simulations of West Nile virus hemifusion (Fig. 4A) (Chao et al., 2014). A hexagonal array of 30 E protomers represents the contact patch between viral and cell membranes (Fig. 4B). Each E subunit transits between an inactive state (in a dimer) and an activated monomer, which can trimerize when two other adjacent monomers are activated. Hemifusion occurs upon formation of two adjacent trimers. Dimer pairs are explicitly defined in the simulation, and a cooperativity factor increases the probability of activation when the dimer partner is already activated. The threshold for trimerization was set to pH 5.4, the bulk threshold for hemifusion, based on our previous finding that these two thresholds are the same for WNV (Chao et al., 2014). The assumption of reversibility for the DV2 E dimer-monomer transition comes from dynamic light scattering measurements performed on Kunjin virus (Chao et al., 2014). The DV2 simulation produced a dwell time histogram at pH 5.5 that could be fit with a single exponential decay (Fig. 4C). In our simulation, the yield for particles achieving hemifusion (defined as the total number of fusion events in a time window divided by the total number of identified particles) was ~25%, as observed experimentally.

We used the DV2 simulation to model action of the small molecule inhibitor by incorporating an inactive, inhibited state into the simulation scheme. Because the simulation explicitly defined the transition, we could inactivate an E protomer at specific steps and monitor the effects on hemifusion yield and dwell times (Fig. 4B). When we “inactivated” DV2 monomers at the trimerization step, we found complete inhibition with ~30 inactive monomers per VLP (Fig. 4D); when we inactivated monomers at the dimer-to-monomer transition, complete inhibition occurred at about ~15 inactive monomers per VLP, in good agreement with the experimental result in Figure 3.

Discussion

The single-particle fusion kinetics for VLPs of all four dengue serotypes are qualitatively similar to those of WNV (Chao et al., 2014). Moreover, explicit simulation of DV2 fusion corresponds to direct experimental observation, for values of the simulation parameters close to those used to fit corresponding data for WNV. The E proteins of WNV and the four serotypes of dengue virus are closely related to each other, and their comparable *in vitro* fusion properties support the robustness of both our experimental design and our fusion model.

Inhibition of dengue virus fusion by 33-110-22, shown previously in bulk assays, confirms its likely mode of action in blocking infection (Schmidt et al., 2012). Synthesis of a fluorescent derivative has enabled us to examine its effects on a single-particle basis and hence to derive not only a bulk inhibitory IC_{50} but to determine the fusion efficiency as a function of the number of molecules bound.

Most of the particles in our preparations were small, 60-subunit (30-dimer) VLPs. The parameter likely to be relevant to small-molecule inhibition is the number of E proteins in the contact zone between particle and target membrane, estimated here, as in our previous work, as 30 -- the extent of a one hemisphere of a small VLP. Assuming that the distribution of bound inhibitor is random, then about 6-7 inhibited monomers in the contact zone (a fractional occupancy of about 0.2) is enough to prevent fusion completely. Our previous work with WNV VLPs showed that virions, virion-sized (180-subunit) VLPs, and small VLPs have indistinguishable fusion kinetics, including their pH dependence (Chao et al., 2014). Therefore, about 35 inhibitors per virion (i.e., about 20% occupancy) should block any detectable fusion, assuming that for complete inhibition the threshold density of bound inhibitor is the same for the two size classes.

Our simulation suggests that 3-110-22 interferes with the dimer-to-monomer activation step at the beginning of the series of fusogenic transitions shown in Fig. 4A. Inhibitor 3-110-22 and its analogs bind the prefusion E dimer before a particle attaches to a cell. They could in principle act at almost any step in the fusion pathway, as they are present even before endocytosis. Their presumptive binding site, the β-octyl glucoside pocket, is at a hinge between domains I and II; the hinge must flex to project the fusion loop outward toward the target membrane. Moreover, the assay that originally identified the cyanohydrazone inhibitors probably worked because they lock the hinge in a dimer-like configuration, even in the context of a fusion-intermediate trimer (Klein et al., 2013). Structural considerations thus reinforce the results of our simulation, that the compounds block the dimer-to-activated-monomer transition.

Materials and Methods

Virus-like particles (VLPs)

Dengue virus-like particles were produced from a stable 293T cell line transfected with the pVRC8400 expression vector with a structural cassette containing a codon-optimized version of the prM-E sequence from the DV 1 clone 45AZ5, DV 2 clone Harvard/BID-V2992/2009, DV 3 isolate IN/BID-V2417/1984, or DV4 isolate TVP/360. A tissue plasminogen activator signal sequence preceded prM-E. DV VLPs were harvested at 28°C from Gibco FreeStyle 293 medium (Life Technologies, Grand Island, NY), clarified from debris by low-speed centrifugation, and precipitated with polyethylene glycol 8000. Following resuspension in buffer containing 20 mM tricine (N-(2-Hydroxy-1,1-bis(hydroxymethyl)ethyl)glycine) pH 7.8, 140 mM NaCl and 0.005% Pluronic F-127, VLPs were purified over an Optiprep density gradient (SW41 rotor, 34,000 rpm, 4°C, 2 hr. 20 min.) with 55%-45%-35%-30%-25%-20–10% steps. We collected the band between the 35% and 30% densities and found this material to contain >95% fully processed M and to contain particles 35 and 50 nm in diameter as assessed by cryo- and negative-stain electron microscopy (Allison et al., 2003). Particles were labeled with DiD (1,1′-dioctadecyl-3,3,3′,3′-tetramethylindodicarbocyanine perchlorate) at ~20 μM or 20-fold the protein concentration. Excess dye was removed using NAP-10 desalting column (GE Healthcare, United Kingdom).

Small molecule synthesis

Synthesis of Alexa fluor 555® conjugate began with phenol installation on 3-110-22 at the 4-position of the benzene ring according to the procedure previously reported (Schmidt et al., 2012). A primary amine with a four-carbon linker was attached to the phenol by etherification and deprotection. Amidation between the primary amine and the commercially available Alexa fluor 555® NHS ester then generated an Alexa fluor 555® conjugated 3-110-22, which was confirmed by ^{1}H NMR.

General SI-Chemistry

All reactions were monitored by LC/MS (Waters 2998 Photodiode Array Detector, Waters SQ detector 2, Waters 515 HPLC pump, Waters 2545 Binary Gradient Module, Waters System Fluidics Organizer and Waters 2767 Sample Manager) using a SunFireTM C18 column (4.6 x 50 mm, 5 µm particle size): solvent gradient = 80% A at 0 min, 1% A at 5 min; solvent A = 0.035% TFA in Water; solvent B = 0.035% TFA in MeOH; flow rate : 1.5 mL/min. Reaction products were purified by flash column chromatography using CombiFlash®Rf with Teledyne Isco RediSep®Rf High Performance Gold or Silicycle SiliaSepTM High Performance columns (4 g, 12 g, 24 g, 40 g, or 80 g) and a Waters HPLC system using SunFireTM Prep C18 column (19 x 100 mm, 5 µm particle size): solvent gradient = 80% A at 0 min, 5% A at 25 min; solvent A = 0.035% TFA in water; solvent B = 0.035% TFA in MeOH; flow rate : 25 mL/min. The purity of all compounds was greater than 95% as analyzed by LC/MS (see above). Chemical shifts are reported below relative to methanol (δ = 3.3) (br = broad, s = singlet, d = doublet, t = triplet, q = quartet, m = multiplet).

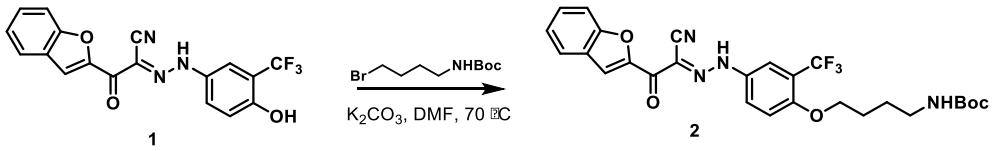

1 2

Compound 1 was prepared from 4-amino-2-(trifluoromethyl)phenol as described (Schmidt et al., 2012. To a solution of compound 1 (250 mg, 0.67 mmol) in *N*,*N*-dimethylformamide (2 mL) were added *tert*-butyl (4-bromobutyl)carbamate (101 mg, 0.40 mmol) and potassium carbonate (139 mg, 1.01 mmol). After stirring at 70 °C for 6 hr, the reaction mixture was cooled to room temperature, diluted with EtOAc and washed five times with water. The organic layer was dried over anhydrous sodium sulfate, filtered, and concentrated under reduced pressure. The residue was purified by flash column chromatography (DCM : MeOH = 90 : 10) to afford compound 2 as a yellow solid (200 mg, 91%). m/z : 567.13 $[M+Na]^{+}$; ^{1}H NMR (600 MHz, CD_3OD) *δ* 7.92 (s, 1H), 7.85 - 7.82 (m, 1H), 7.80 (d, *J* = 7.6 Hz, 1H), 7.77 - 7.73 (m, 1H), 7.63 (d, *J* = 8.8 Hz, 1H), 7.54 (t, *J* = 7.6 Hz, 1H), 7.37 (t, *J* = 7.3 Hz, 1H), 7.29 (d, *J* = 9.4 Hz, 1H), 4.14 (t, *J* = 6.2 Hz, 2H), 3.11 (t, *J* = 6.8 Hz, 2H), 1.87 - 1.81 (m, 2H), 1.71 - 1.64 (m, 2H) 1.43 (s, 9H).

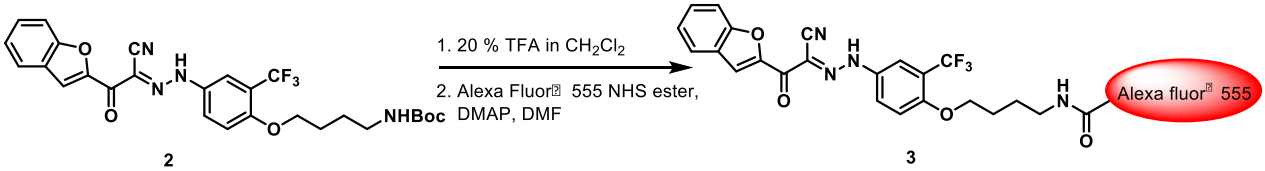

2 3

Step 1 : To a solution of compound 2 (200 mg, 0.37 mmol) in CH2Cl2 (4 mL) was added trifluoroacetic acid (1 mL). After stirring for 1 hr, the reaction mixture was diluted with CH2Cl2 and alkalinized with saturated sodium bicarbonate. The organic layer was separated, and the aqueous layer was extracted five times with CH_2Cl_2. The combined organic layer was dried over anhydrous sodium sulfate, filtered and concentrated under reduced pressure to give N-Boc deprotected precursor as a yellow oil (152 mg, 92%) m/z : 445.07 [M+1]+.

Step 2 : To a solution of compound 2 (2.7 mg, 0.006 mmol) in *N*,*N*-dimethylformamide (0.5 mL) were added DMAP (0.6 mg, 0.0048 mmol) and Alexa fluor 555 NHS ester (ThermoFisher Scientific, m.w. ~ 1250, 5 mg, 0.004 mmol). The resulting mixture was stirred at room temperature for 3 hr, diluted with DMSO and the product purified by prepHPLC to give compound 3 as a red solid (m.w. ~1579, 1.5 mg, 24%).

Single Particle Assay

Single particle data were collected as previously described (Chao et al., 2014). Briefly, glass coverslips were cleaned by sonication in '7X' detergent, 1M potassium hydroxide, acetone and ethanol, and dried for 1 hr at 100°C. Polydimethylsiloxane (PDMS) flow cells with 0.5 mm wide and 70 µm high channels (5 per cell) were bonded to plasma-treated glass. Teflon FEP tubing (0.2 mm, Upchurch Scientific) connected an Eppendorf tube with solution to the channel, and Intramedic polyethylene tubing (0.76 mm) connected the channel to a syringe pump (Harvard Pump 11; Harvard Apparatus, Holliston, MA).

Liposomes for preparing planar bilayers contained 1-palmitoyl-2-oleoyl-sn-glycero-3-phosphoethanolamine (POPE), 1-oleoyl-2-palmitoyl-sn-glycero-3-phosphocholine (POPC), cholesterol, and 1,2-dioleoyl-sn-glycero-3-phosphocholine (DOPC), 1,2-dioleoyl-sn-glycero-3-phosphoethanolamine-N-(carboxyfluorescein) (FL-PE) and 1,2-dioleoyl-sn-glycero-3-[(N-(5-amino-1-carboxypentyl)iminodiacetic acid)succinyl] (Ni-NTA DOGS) (Avanti Polar Lipids, Alabaster, AL) in a ratio of 4:2:2:2:0.02:1%. Liposomes at 10 mg/ml were extruded through a 200 nm pore-size polycarbonate membrane filter. Liposomes were loaded into the flow cell, and the flow stopped to allow bilayers to form. We performed fluorescence recovery after photobleaching experiments to confirm the fluidity of the bilayer. Unattached liposomes were washed away, and 1A1D-2 Fab or the lectin domain of DCSIGN-R, with a C-terminal His6 tag, was introduced at 50 nM for 2 min. 1A1D-2 Fab was produced from a stable 293T line expressing both heavy and light chains from the pVRC8400 vector, purified by Ni-affinity chromatography and S200 size-exclusion chromatography. DCSIGN-R was expressed from Hi-5 cells infected with recombinant baculovirus. Labeled virus particles were loaded onto the pseudo-receptor decorated bilayer. To initiate fusion, we introduced acetate buffer (100 mM sodium acetate, pH 5.0–5.5) or MES (100 mM, pH 5.75–6.25), with 140 mM sodium chloride and 0.005% Pluronic F-127.

Fluorescence measurements

End-point bulk fusion data were collected using a GE Amersham Typhoon plate reader at 633 nm and 670 nm excitation and emission wavelengths respectively in 96-well clear-bottom plates with 2 mg/ml final lipid concentration (200 nm liposomes prepared as described above). VLPs were prepared and labeled with DiD as previously described (Chao et al., 2014).

Bulk liposome fusion data were collected on a PTI (Photon technology International, Edison, NJ) 814 Fluorimeter, with 648 nm and 669 nm excitation and emission wavelengths respectively, using a Cole–Parmer digital polyStat temperature controlled thermo-jacket at 2 Hz over 10 min and at 0.2 mM final lipid concentration (200 nm liposomes prepared as described above).

Single-particle fusion data were collected on an inverted Olympus IX71 fluorescence microscopy with a high numerical aperture objective (60×, N.A. = 1.3). VLPs were illuminated with 488 and 640-nm Coherent (Wilsonville, OR) lasers. A custom-fabricated water-chilled temperature collar (Bioptecs, Butler, PA) was fitted on the objective turret. Each time-lapsed fluorescence video was recorded at 1 Hz for 300 s using 3i Slidebook software. Data were analyzed using Igor and MatLab. IC_{50} was determined by non-linear regression.

The single-fluorophore fluorescence intensity was calibrated by drying buffer containing the labeled small molecule onto a glass slide and monitoring single step photobleaching events under identical imaging conditions as in the experiment.

Competition assay

We used TIRF microscopy, as described (Chao et al., 2014). Coverslips were sonicated in ethanol and water and then glow discharged prior to use. VLPs were dye labeled as in fusion experiments, but at 1:10 the concentration of DiD as we did not require quenching; the concentration of VLPs was 5 times higher than used for the bulk fusion assay. Labeled VLPs were mixed with 1μM fluorescent inhibitor for 5 mins before loading onto the TIRF. For competition assays with unlabeled inhibitor, DiD labeled VLPs were first incubated with the 3-110-22 for 5 mins at 1 or 10μM, followed by addition of Alexa555/3-110-22 for 5 mins. Calcuations were made by densitometry of the VLP spots as identified in ImageJ. The spots were found with the VLP fluorescent channel (DiD) and then both channels were measured, background subtracted, and the ratio of Alexa555 to DiD determined.

Simulations

Matlab code, modified from our previous work (Chao et al., 2014), was used with parameters optimized against experimentally measured values for DV2. Code is publicly available at https://github.com/Harrison-Lab/Flavivirus.

Acknowledgments

We thank Ilya Kuesters and T. Kirchhausen (Boston Children's Hospital) for assistance with TIRF microscopy and access to facilities. LHC was a Frederic M. Richards Fellow of the Jane Coffin Childs Memorial Fund for Medical Research and Charles King Trust Fellow. AN was supported by the Howard Hughes Medical Institute EXROP program. SCH is an investigator in the Howard Hughes Medical Institute. We acknowledge support from NIH grants CA13202 and AI109740 (Center for Excellence in Translational Research).

Additional information

Competing interests: The authors declare no competing interests.

Funding:

NIH	CA13202	Stephen C. Harrison
NIH	AI109740	Stephen C. Harrison, Nathanael S. Gray, Priscilla L. Yang
HHMI		Stephen C. Harrison
Jane Coffin Childs Memorial Fund for Medical Research		Luke H. Chao
Charles King Trust		Luke H. Chao

Author contributions

LHC, conception and design,acquisition of data, analysis and interpretation of data, design and writing of simulation code, drafting and revising manuscript; JJ, design and synthesis of Alexa555/3-110-22; AJ, experimental design, acquisition and analysis and interpretion of data; AN, acquisition of data; NSG: conception and design, revision of manuscript; PLY, conception and design, revision of manuscript; SCH: conception and design, analysis and interpretation of data, drafting and revising manuscript.

Figure captions

Fig. 1. Fusion measurements. A. Fusion (with liposomes, in bulk solution) for VLPs of the four DV serotypes. The fluorescence from membrane-incorporated DiD is shown as a function of pH. Hemifusion (or fusion) at low pH causes dequenching of the VLP-incorporated fluorophore. B. Histograms of single-particle fusion dwell times (between lowering of pH and observed dequenching) at pH 5.5 for each of the four DV serotypes. Curves show fit with a single exponential (DV1, DV2, and DV4) or with a gamma distribution, N=2 (DV3).

Fig. 2. Inhibition of DV2 VLP fusion by 3-110-22. A. Fluorescence dequenching as a function of inhibitor concentration. B. Single-particle dwell-time distribution at pH 5.5 in the presence of 1 μM inhibitor. Fig. 2 -- figure supplement 1. Inhibition of DV2 VLP fusion by Alexa-555/3-110-22.

Fig 2 -- figure supplement 1. Inhibition of DV2 VLP fusion by Alexa-555/3-110-22. A. Fluorescence dequenching as a function of inhibitor concentration. Percent dequenching calculated with 100% as DiD dequenching with no added inhibitor and 0% as dequenching with no pH drop. Error bars are SEM, n=3. B. Single-particle binding intensity for Alexa-555/3-110-22 in the presence of varying molar ratios of underivatized 3-110-22 (none, 1:1, 1:10). Error bars: SEM; n=373, 370, 382 for the three sets of measurements, respectively.

Fig. 3. Single-particle hemifusion as a function of number of bound Alexa-fluor-555/3-110-22 molecules. Hemifusion measured as DiD fluorescence dequenching. Histogram shows the number of particles with a particular number of bound fluorescent inhibitor molecules, in bins of five. Number of paticles in the bin that did not fuse in the time of the experiment in blue (total height of bar); number of fusing particles, in purple.

Fig. 4. Simulation of the effects of inhibitor, as a function of the number of bound molecules (assuming that an inhibitor blocks activity of the monomer to which it binds). A. Overall scheme of the fusion transition (Chao et al., 2014). The structures at the left show the E prefusion dimer, its packing on the virion, and the E postfusion trimer. B. Representation of a contact zone with 30 monomers. In the simulations of 3-110-22 inhibition, variable numbers of E subunits were inactivated, illustrated here, for 10 bound inhibitors in the contact zone, as dark crosses. The number of ways (2) of forming two adjacent trimers from three active monomers is much smaller than it is with all monomers active (76). C. Comparison of simulation and experiment, for single-particle measurements of DV2 fusion. The left-hand panel is the same as the second panel in Fig. 2. The right-hand panel shows the results of a simulation with parameters as described in the text. D. Simulation results for two alternative inhibition points: blocking extension of the monomer (orange) or inactivating foldback of a trimer (red). Agreement with the data in Fig. 3 favors the former model.

References

Chao, L.H., Klein, D.E., Schmidt, A.G., Pena, J.M., and Harrison, S.C. (2014). Sequential conformational rearrangements in flavivirus membrane fusion. eLife *4*.
Clark, M.J., Miduturu, C., Schmidt, A.G., Zhu, X., Pitts, J.D., Wang, J., Potisopon, S., Zhang, J., Wojciechowski, A., Hann Chu, J.J.*, et al.* (2016). GNF-2 Inhibits Dengue Virus by Targeting Abl Kinases and the Viral E Protein. Cell Chem Biol *23*, 443-452.
Diamond, M.S., and Pierson, T.C. (2015). Molecular Insight into Dengue Virus Pathogenesis and Its Implications for Disease Control. Cell *162*, 488-492.
Floyd, D.L., Ragains, J.R., Skehel, J.J., Harrison, S.C., and van Oijen, A.M. (2008). Single-particle kinetics of influenza virus membrane fusion. Proc Natl Acad Sci U S A *105*, 15382-15387.
Harrison, S.C. (2015). Viral membrane fusion. Virology *479-480*, 498-507.
Heinz, F.X., and Stiasny, K. (2012). Flaviviruses and flavivirus vaccines. Vaccine *30*, 4301-4306.
Ivanovic, T., Choi, J.L., Whelan, S.P., van Oijen, A.M., and Harrison, S.C. (2013). Influenza-virus membrane fusion by cooperative fold-back of stochastically induced hemagglutinin intermediates. eLife *2*, e00333.
Kim, I.S., Jenni, S., Stanifer, M.L., Roth, E., Whelan, S.P., van Oijen, A.M., and Harrison, S.C. (2017). Mechanism of membrane fusion induced by vesicular stomatitis virus G protein. Proc Natl Acad Sci U S A *114*, E28-E36.
Klein, D.E., Choi, J.L., and Harrison, S.C. (2013). Structure of a dengue virus envelope protein late-stage fusion intermediate. J Virol *87*, 2287-2293.
Lok, S.M., Kostyuchenko, V., Nybakken, G.E., Holdaway, H.A., Battisti, A.J., Sukupolvi-Petty, S., Sedlak, D., Fremont, D.H., Chipman, P.R., Roehrig, J.T.*, et al.* (2008). Binding of a neutralizing antibody to dengue virus alters the arrangement of surface glycoproteins. Nat Struct Mol Biol *15*, 312-317.
Modis, Y., Ogata, S., Clements, D., and Harrison, S.C. (2003). A ligand-binding pocket in the dengue virus envelope glycoprotein. Proc Natl Acad Sci U S A *100*, 6986-6991.
Modis, Y., Ogata, S., Clements, D., and Harrison, S.C. (2004). Structure of the dengue virus envelope protein after membrane fusion. Nature *427*, 313-319.
Rey, F.A., Heinz, F.X., Mandl, C., Kunz, C., and Harrison, S.C. (1995). The envelope glycoprotein from tick-borne encephalitis virus at 2 A resolution. Nature *375*, 291-298.
Schmidt, A.G., Lee, K., Yang, P.L., and Harrison, S.C. (2012). Small-molecule inhibitors of dengue-virus entry. PLoS Pathog *8*, e1002627.
Tassaneetrithep, B., Burgess, T.H., Granelli-Piperno, A., Trumpfheller, C., Finke, J., Sun, W., Eller, M.A., Pattanapanyasat, K., Sarasombath, S., Birx, D.L.*, et al.* (2003). DC-SIGN (CD209) mediates dengue virus infection of human dendritic cells. J Exp Med *197*, 823-829.

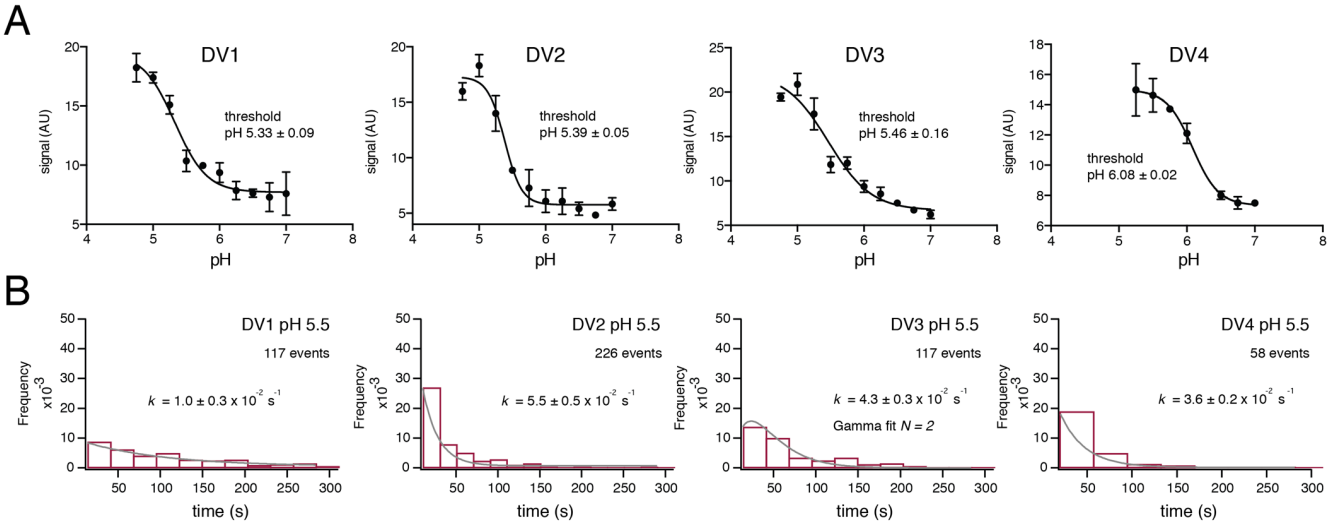

Fig. 1

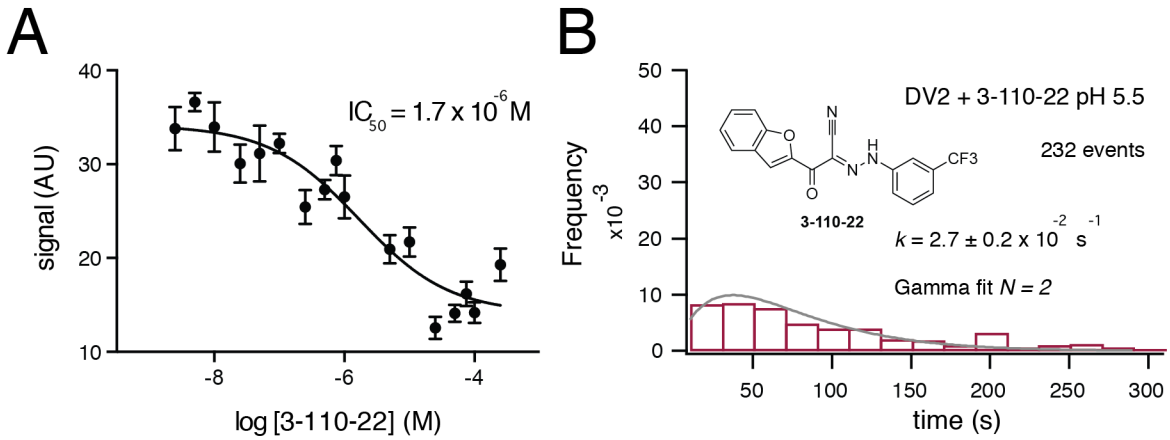

Fig. 2

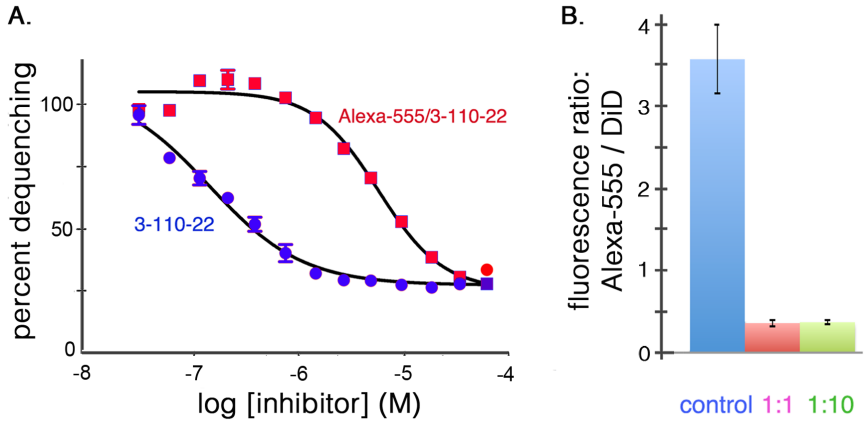

Fig. 2 -- figure supplement 1

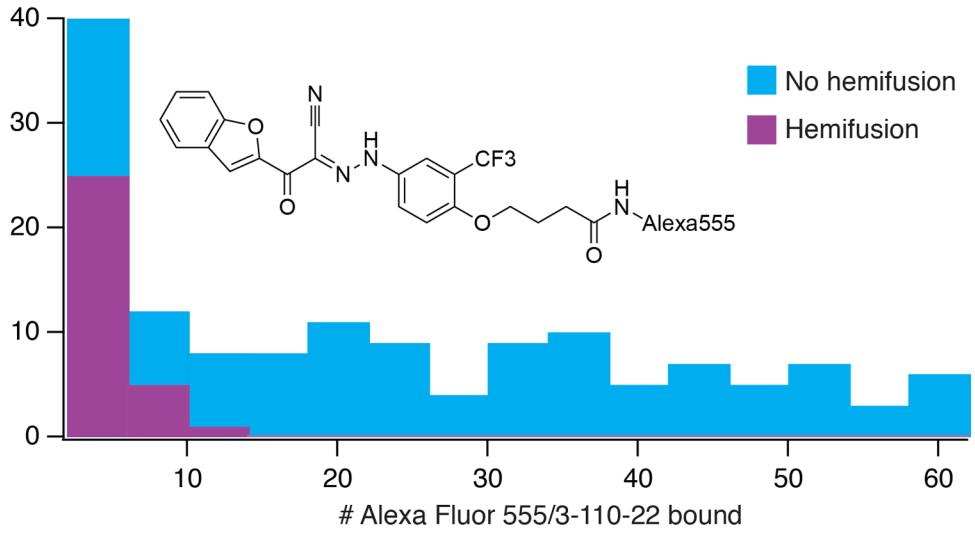

Fig. 3

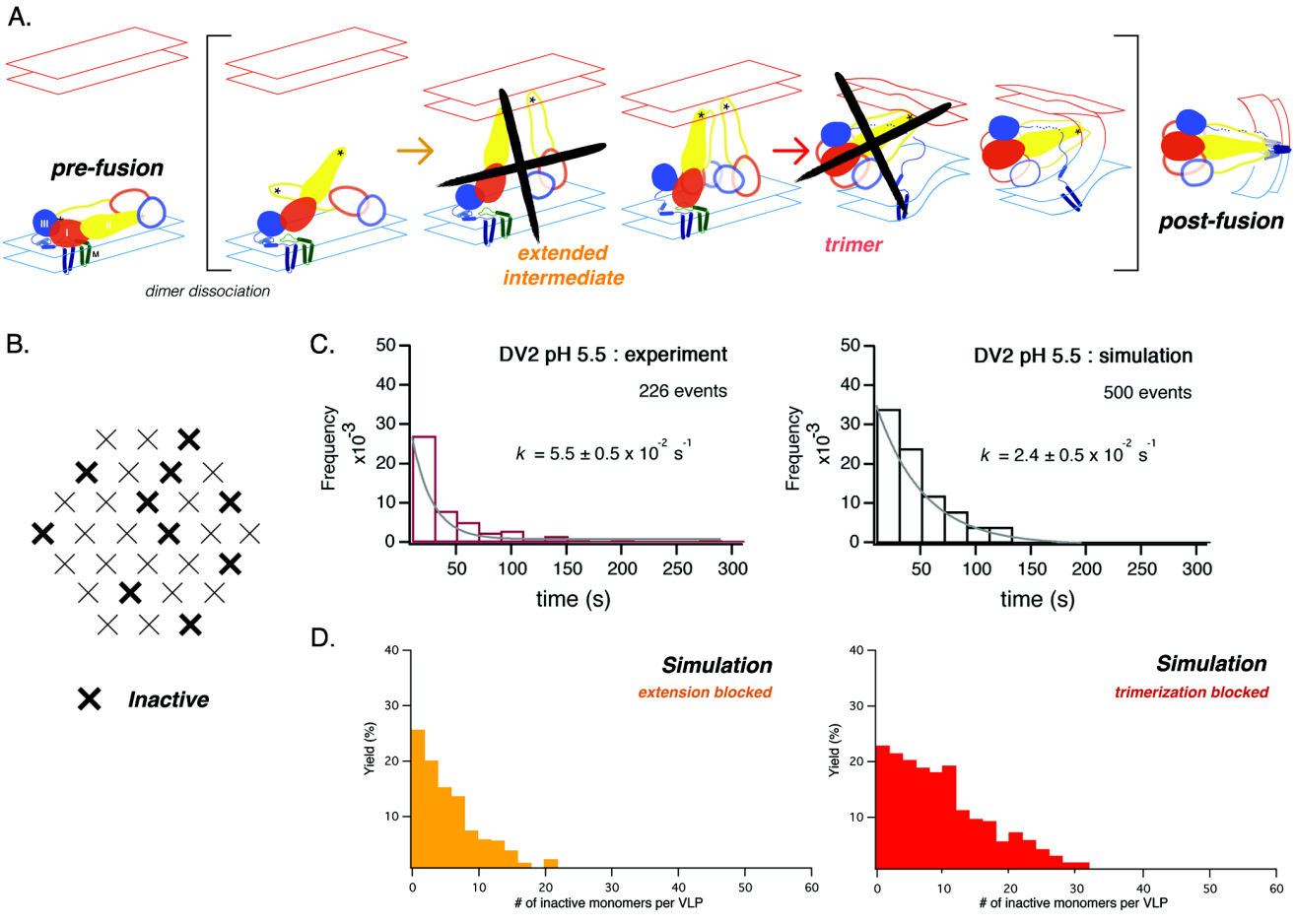

Fig. 4